JOURNAL OF SOLID STATE CHEMISTRY 116, 185–192 (1995)

Impedance-Spectroscopy Analysis of a $LiTaO_3$-Type Single Crystal

Dong Ming,* J. M. Reau,* J. Ravez,* Joo Gitae,† and P. Hagenmuller*

*Laboratoire de Chimie du Solide du CNRS, Université de Bordeaux I, 351 cours de la Libération, 33405 Talence Cedex, France; and †KIST, P.O. Box 131, Cheongryang, Seoul, Korea

Received July 1, 1994; in revised form October 17, 1994; accepted October 19, 1994

Low-frequency dielectric dispersion phenomena in a $LiTaO_3$-type single crystal have been analyzed by impedance spectroscopy in directions parallel and perpendicular to the polar *c*-axis (rhombohedral system). An empirical expression has been deduced for the complex permittivity $\varepsilon^*(\omega)$,

$$\varepsilon^*(\omega) = \varepsilon_\infty + \frac{\varepsilon_s - \varepsilon_\infty}{1 + (i\omega/\omega_1)^m} + \frac{\sigma_0}{\varepsilon_0\omega}[1 + (i\omega/\omega_2)^n],$$

where the (ω_1, m) and (ω_2, n) couples characterize respectively the lattice and the charge carrier responses. This relation may be considered as a generalization of the Cole–Cole dielectric expression [*J. Chem. Phys.* 9, 341 (1941)]. Excellent agreement has been obtained in a wide frequency domain (1–10^6 Hz) between the measured and calculated permittivities in the 500–650°C temperature range (T_C = 600°C). The temperature dependence of various dielectrical parameters has been determined and discussed. The relaxations are correlated to Li atom motions.

1. INTRODUCTION

$LiTaO_3$-type ferroelectrics have very good electrooptic properties and are technologically important for electrooptic, electroacoustic, and nonlinear devices (2). Structural and dielectric investigations have shown the existence of a $Li_{1-5x}Ta_{1+x}O_3$ solid solution with a systematic reduction of the ferroelectric Curie temperature, T_C, as the Li/Ta ratio decreases (3). The presence of lithium vacancies within the solid solution allows the simultaneous occurrence of ferroelectric and ionic conductivity properties; as a matter of fact, fixed frequency measurements of ε_r' with temperature for nonstoichiometric compositions show a strong low-frequency dielectric dispersion in the neighborhood of T_C (4). In the present paper, the low-frequency dielectric dispersion of a nonstoichiometric $LiTaO_3$ crystal was measured in directions parallel and perpendicular to the polar *c*-axis (rhombohedral system) using impedance spectroscopy.

2. EXPERIMENTAL

A lithium-deficient $LiTaO_3$ crystal was prepared by the Czochralski method; a Curie temperature of 600°C was consistent with a composition described by $Li_{0.980}Ta_{1.004}O_3$ (3).

Sample 1 (Z-cut) was a 10 × 10 × 1.56 mm parallelepiped, the large face being perpendicular to the polar axis. Sample 2 (X-cut) was disk-shaped (0.9 mm thick and 24 mm in diameter), a diameter being parallel to the polar axis. Pt paste electrodes (circular, 8 mm in diameter) were deposited on opposing faces of the cut crystals.

Impedance measurements were carried out in dry helium upon heating. At each interval, the sample temperature was maintained by a Eurotherm-902 S controller for 0.5 hr before collecting data; the stability was ± 0.5°C. A frequency sweep from 10^6 to 1 Hz (61 frequency points, logarithmic scale 6.0 to 0.0) with a nominal applied voltage of 500 mV) was achieved using a Solartron-1260 Impedance Gain Phase Analyzer.

3. RESULTS

3.1. The ac Complex Impedance Results

Typical complex plane plots, ρ'' vs ρ', are shown in Fig. 1 for both samples, i.e., $\rho^* = Z^*(S/d) = \rho' - i\rho''$, where ρ is the ac resistivity, S is the area of the Pt electrode, and d is the separation between electrodes.

The low-frequency response appears as an inclined spike and is characteristic of a blocking double layer capacitance, C_{dl}. The values for such capacities, assuming $Z'' = 1/2\pi fC_{dl}$, are about 6 μF. These values are typical of those expected for the blocking of ionic charge carriers at electrode–electrolyte interfaces (4). These results exhibit Li^+ conduction in both samples oriented along directions either parallel or perpendicular to the polar axis. The Li^+ conductivity in the polar axis direction (sample 1) is a little greater than in the direction perpendicular to the polar axis (sample 2).

In the temperature range close to T_C (595–615°C), the data corresponding to sample 2 show a tendency to split into two semicircles. Since the sample is a single crystal, this behavior suggests the possible occurrence of two dispersion mechanisms.

Figure 2 displays the variation of log Z'' with log f for

0022-4596/95 $6.00

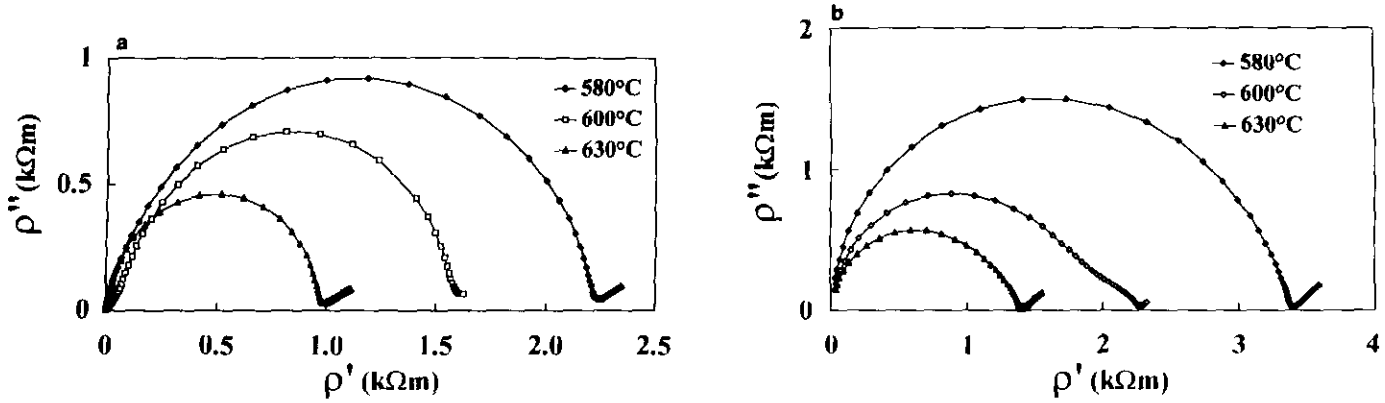

FIG. 1. Complex plane plots of (a) sample 1 and (b) sample 2.

three typical temperatures. At temperatures close to T_C, the high-frequency slope for sample 1 and the low-frequency for sample 2 are not straight lines, which further suggests the presence of several dispersion mechanisms for both samples.

3.2. *Frequency Dependence of the Permittivities* $\varepsilon_r'(meas)$ *and* $\varepsilon_r''(meas)$

Electrical data measured as an impedance, Z^*, have been converted into permittivity, ε^*, using the relation

$$\varepsilon^* = 1/i\omega C_0 Z^*, \qquad [1]$$

where C_0 is the vacuum capacitance (5).

The frequency dependence of the permittivities ε_r' (meas) and ε_r''(meas) is shown in Figs. 3 and 4 for five typical temperatures using a double logarithmic scale.

The variation of ε_r'(meas) with frequency for sample 1 (Fig. 3a) has the following features:

—for $T \ll T_C$ and $T \gg T_C$, two domains can be observed: a high-frequency region ($f \gtrsim 10^3$ Hz), where ε_r'(meas) is nearly frequency independent, and a low-frequency region ($f \lesssim 10$ Hz), where ε_r'(meas) rises strongly with decreasing frequency.

—for temperatures close to T_C, two frequency-independent regimes are clearly evident, the first at about 10^3 Hz and the second above 10^5 Hz. As $|T - T_C|$ becomes smaller, the first region shifts progressively toward lower frequencies.

The variation of ε_r''(meas) with frequency of sample 1 (Fig. 3b) has a behavior similar to that of ε_r'(meas); how-

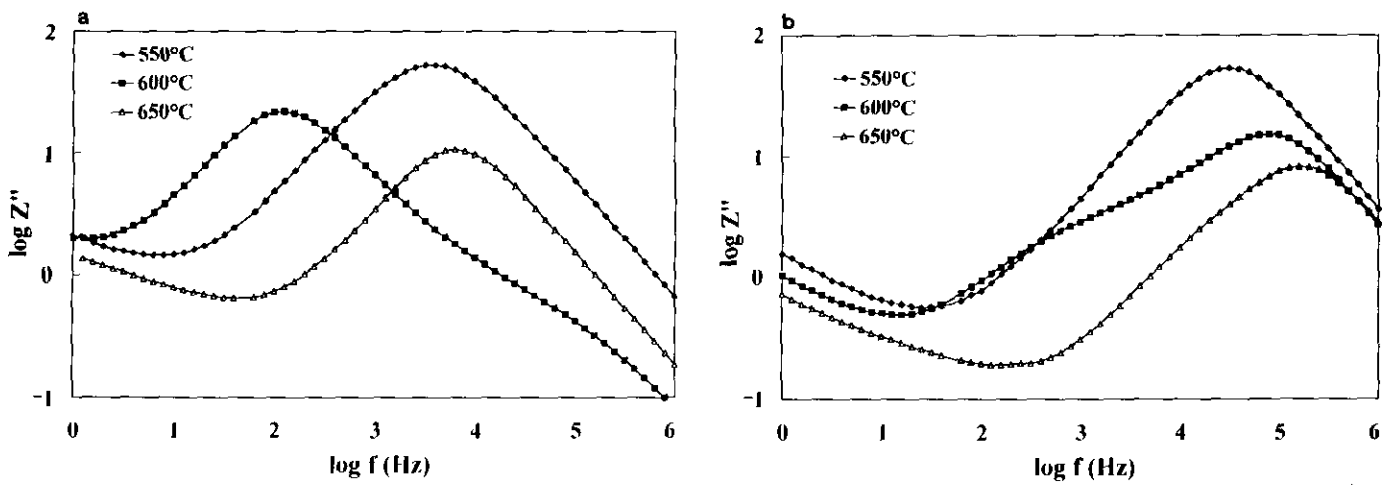

FIG. 2. Variation of log z'' with log f at various temperatures for (a) sample 1 and (b) sample 2 (the curves drawn through the reported data are visual guides).

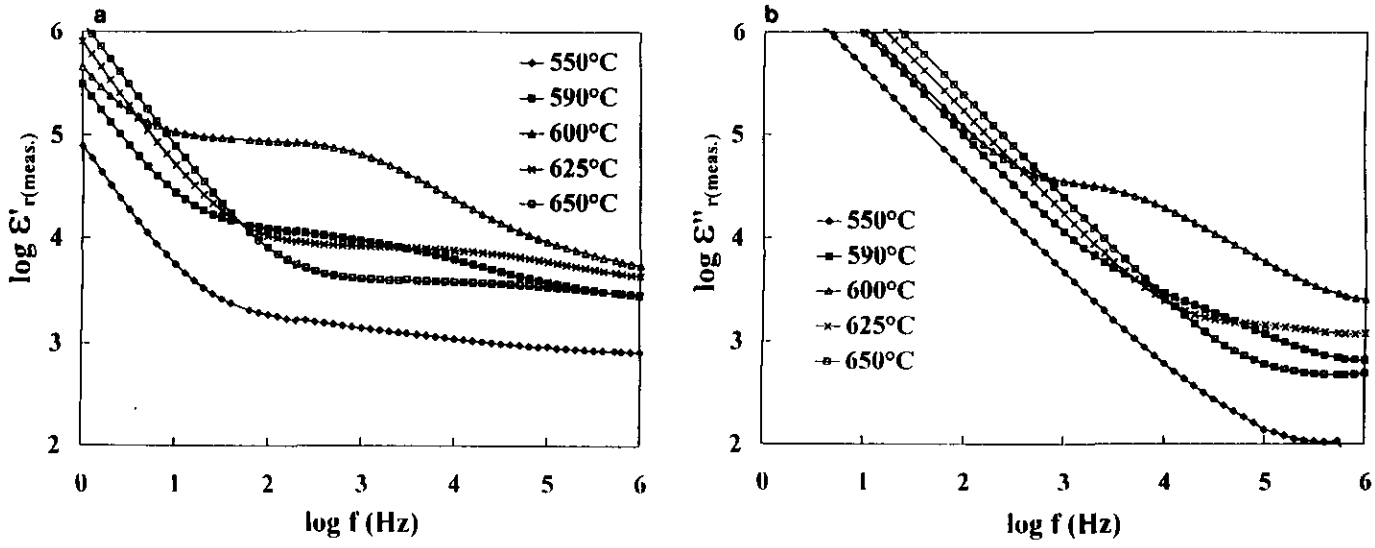

FIG. 3. Variation of (a) log ε_r'(meas) and (b) log ε_r''(meas) with log f at different temperatures for sample 1 (the curves drawn through the reported data are visual guides).

ever, the frequency-independent region observed at high frequency appears at somewhat higher frequencies, above 10^5 Hz, and the frequency-dependent region is correspondingly wider. In addition, the second frequency-independent region at $T \simeq T_C$ is narrower (10^3–10^4 Hz).

For sample 2, the behavior of ε_r'(meas) (Fig. 4a) is similar to that of sample 1 but is less pronounced. In contrast, the data of ε_r''(meas) (Fig. 4b) exhibit a nearly linear dependence on frequency up to ca. 10^5 Hz.

4. DISCUSSION

4.1. Dielectric Dispersion Model

The complex permittivity of a Debye-type ideal material is described by the Cole–Cole expression (1),

$$\varepsilon^*(\omega) = \varepsilon_\infty + \frac{\varepsilon_s - \varepsilon_\infty}{1 + i\omega/\omega_1}, \qquad [2]$$

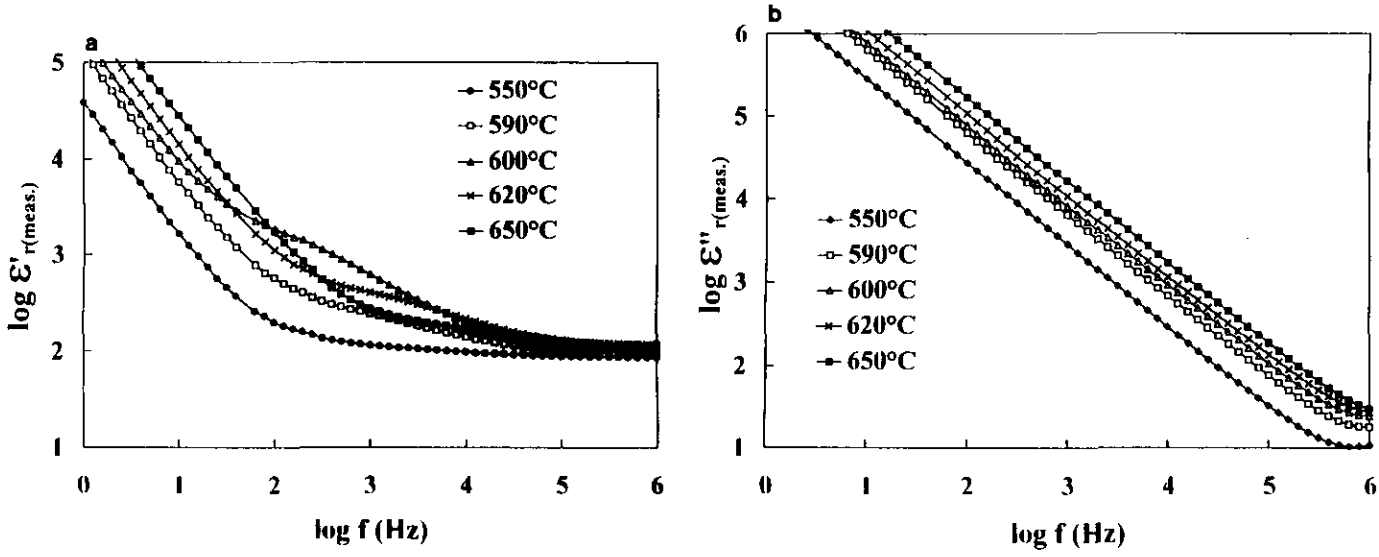

FIG. 4. Variation of (a) log ε_r'(meas) and (b) log ε_r''(meas) with log f at different temperatures for sample 2 (the curves drawn through the reported data are visual guides).

where ε_s is the static permittivity, ε_∞ is the permittivity at "infinitely" high frequency, and ω_1 is the relaxation angular frequency of the Debye process.

The behavior of most dielectric materials deviates from the Debye response and is often described by a modified espression, such as

$$\varepsilon^*(\omega) = \varepsilon_\infty + \frac{\varepsilon_s - \varepsilon_\infty}{1 + (i\omega/\omega_1)^{1-\alpha}}, \quad [3]$$

where graphically, the parameter α represents the tilting angle ($\alpha\pi/2$) of the circular arc from the real axis in the complex-permittivity plane.

On the other hand, for ionic conducting materials, the conductivity frequency-dependence can be represented by the Almond–West expression (6),

$$\sigma^*(\omega) = \sigma_0[1 + (i\omega/\omega_2)^n], \quad [4]$$

where σ_0 is the dc conductivity, ω_2 is the ionic hopping angular frequency, and n is a dimensionless exponent ($0 < n < 1$).

Since long-range Li^+ diffusion occurs in these ferroelectric crystals, two polarization mechanisms are possible, namely:

(i) the dielectric relaxation (or lattice response) due to permanent dipole orientations or other motions which do not involve long-range displacement of mobile charge carriers, characterized by ω_1 and m, where $m = 1 - \alpha$, and

(ii) the conductivity relaxation, or carrier response, associated with long range migration described by ω_2 and n.

Consequently, $\varepsilon^*(\omega)$ may be described as follows:

$$\varepsilon^*(\omega) = \varepsilon^*(\omega)_{(\text{latt})} + \varepsilon^*(\omega)_{(\text{carr})}$$
$$\varepsilon^*(\omega) = \varepsilon_\infty + \frac{\varepsilon_s - \varepsilon_\infty}{1 + (i\omega/\omega_1)^m} + \frac{\sigma_0}{\varepsilon_0\omega}[1 + (i\omega/\omega_2)^n]. \quad [5]$$

The complex permittivity may be decomposed into real and imaginary parts, i.e.,

$$\varepsilon^*(\omega) = \varepsilon_r' - i\varepsilon_r'',$$

where

$$\varepsilon_r' = \varepsilon_\infty + \frac{(\varepsilon_s - \varepsilon_\infty)[1 + (\omega/\omega_1)^m \cos(m\pi/2)]}{1 + 2(\omega/\omega_1)^m \cos(m\pi/2) + (\omega/\omega_1)^{2m}} + \frac{\sigma_0}{\varepsilon_0\omega}(\omega/\omega_2)^n \sin(n\pi/2) \quad [6]$$

and

$$\varepsilon_r'' = \frac{(\varepsilon_s - \varepsilon_\infty)(\omega/\omega_1)^m \sin(m\pi/2)}{1 + 2(\omega/\omega_1)^m \cos(m\pi/2) + (\omega/\omega_1)^{2m}} + \frac{\sigma_0}{\varepsilon_0\omega}[1 + (\omega/\omega_2)^n \cos(n\pi/2)]. \quad [7]$$

Analysis of the experimental data was carried out on the basis of Eqs. [6] and [7] using the simplex method (7). The parameters σ_0, m, n, ω_1, ω_2, ε_s, and ε_∞ were obtained from a best fit to both ε_r' and ε_r''. The calculated σ_0 values were in good agreement with those obtained by extrapolating the inclined spike to the real Z'-axis in the complex plane; cf. Figs. 1a and 1b. Typical fitting results are shown in Figs. 5a and 5b for samples 1 and 2, respectively. The disagreement between the measured and calculated values for ε_r' at low frequencies is likely due to electrode effects, as previously noted.

The excellent agreement between experimental and calculated data over a wide frequency range for both ε_r' and ε_r'' is consistent with the proposed model for our crystals.

4.2. Influence of Temperature on the Various Parameters

4.2.1. The dc conductivity σ_0. Figure 6 exhibits the variation of log σ_0 vs reciprocal temperature for samples 1 and 2. The conductivity is somewhat higher, ca. factor 2, the activation energy slightly lower in the polar axis direction than in directions perpendicular to this axis; ΔE_σ (Z-cut) = 1.10 eV, ΔE_σ (X-cut) = 1.20 eV. No anomaly, such as a slope change, is manifested at T_C.

4.2.2. The exponents m and n. The temperature dependence of the exponents m and n is illustrated in Figs. 7a and 7b for samples 1 and 2, respectively.

Sample 1 exhibits the following features over the investigated temperature range:

—in the ferroelectric state, m and n increase with increasing temperature;

—at $T \simeq T_C$, there is a maximum of m and a corresponding minimum in n;

—in the paraelectric state, m again increases with increasing temperature, whereas n does not depend significantly on temperature.

Sample 2 is characterized by the following features:

—m decreases with rising temperature except at the phase transition region where a local maximum occurs at T_C;

—n is close to 1 below and above the transition region, but a minimum of n appears at T_C.

For both samples, the values of n are close to 1 ($0.8 \lesssim n \lesssim 1$), and the values of m are smaller than those of n in the temperature range considered here. Consequently,

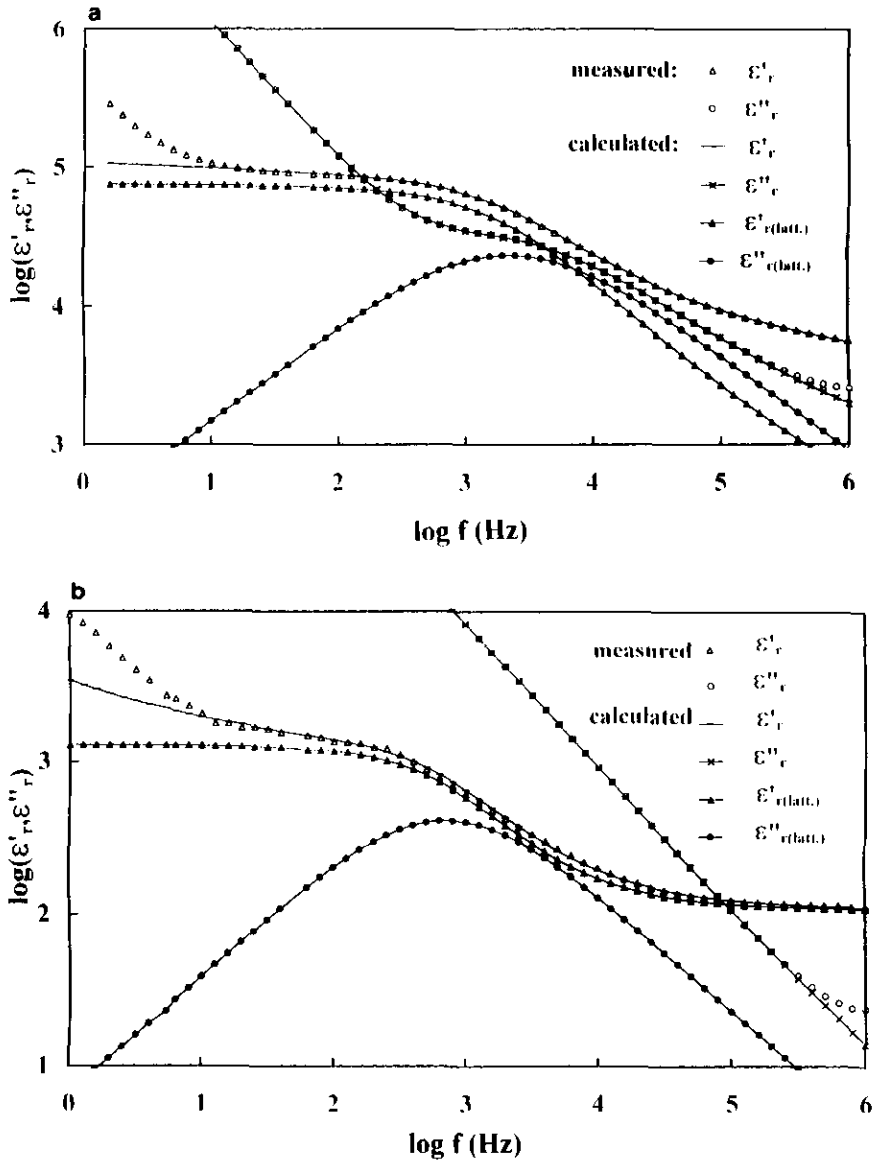

FIG. 5. Experimental results and model calculations (—) of log (ε_r', ε_r'') with log f at 600°C for (a) sample 1 and (b) sample 2.

the carrier polarization mechanism is weakly dispersive, while the lattice polarization mechanism is somewhat more dispersive. Furthermore, both samples are characterized by a maximum in m and a minimum in n at T_C; a compensation effect seems to appear at T_C between dispersions of the two polarization processes.

The sudden drop of n in the temperature range close to T_C may suggest that the carrier polarization mechanism is coupled with a soft mode (8) according to the lattice dynamic theory (9); i.e., a transverse optical dynamic mode is softened, and the restoring force tends to zero at the ferroelectric–paraelectric phase transition. This phenomenon requires a higher energy loss and a concomitant smaller energy storage; consequently, a minimum in n occurs at T_C in accordance with Jonscher's relation (10):

$$\text{lost energy/stored energy} = \text{cost } (n\pi/2).$$

4.2.3. The characteristic frequencies f_1 and f_2. The temperature dependences of f_1 and f_2 ($f = \omega/2\pi$) are plotted in Figs. 8a and 8b for samples 1 and 2, respectively.

For sample 1, minima in f_1 and f_2 are clearly visible at T_C, where a minimum in n has already been noted. This result suggests that, as the crystal temperature approaches T_C, a longer time is required for relaxation after perturbation. The simultaneous existence of minima in n, f_1 and t_2, at T_C suggests, according to the soft-mode theory (9), that the lattice and carrier relaxations are coupled to the soft mode.

A comparative study of the temperature dependence of f_1 and f_2 gives the following results:

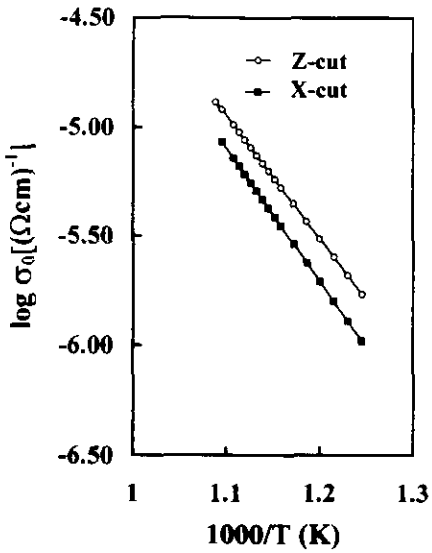

FIG. 6. Temperature dependence of log σ_0 for both samples.

—For temperatures lower than T_C–25°C, f_1 increases and f_2 decreases with rising temperature, the difference $|f_1 - f_2|$ becomes progressively smaller with increasing T.

—For T_C–25°C $\lesssim T \lesssim T_C$, f_1 is larger than f_2; however, the magnitudes of these quantities are the same.

—For $T \gtrsim T_C$, both f_1 and f_2 increase. The characteristic frequency, f_1, is larger than f_2, and the difference in $|f_1 - f_2|$ increases with rising temperature.

The lattice relaxation frequency f_1 is related to an intrinsic polarization process. In other words, in the ferroelectric state, as T approaches T_C, the spontaneous polarization mechanism involves a temperature dependence analogous to the f_2 relaxation frequency of the charge carriers. Consequently, in this temperature range, the lattice polarization and carrier polarization mechanisms become increasingly correlated. In the paraelectric state, on the other hand, the two mechanisms become progressively more independent with rising temperature.

For sample 2, the temperature dependence of f_1 and f_2 is weak, and only a shallow minimum at T_C is apparent for each characteristic frequency (Fig. 8b). Additionally, f_2 is larger than f_1, and the quantity $|f_1 - f_2|$ is sufficiently large to assume that the two polarization mechanisms are actually independent from each other in the temperature range considered.

Both relaxations are related to Li atom motions through an octahedron face:

—The lattice relaxation is correlated to short-range lithium displacements along the polar axis across an oxygen triangle common to two octahedra. These backward and forward motions are partially responsible for the inversion of the ferroelectric spontaneous polarization. The minimum of f_1 at T_C corresponds to the largest displacements due to the decrease of bond strength (soft mode).

—The carrier relaxation is due to Li^+ ionic conductivity. Such a long-range effect is intensified by the lithium vacancies in the $LiTaO_3$-type network of crystals investigated.

4.2.4. The static permittivity ε_s and the permittivity at "infinitely" high frequency ε_∞. The temperature dependence of ε_s appears in Fig. 9 for both samples. For sample 1, ε_s exhibits a sharp peak at T_C. In contrast, only a little peak is observed for sample 2. Since the spontaneous polarization process takes place along the polar axis, the

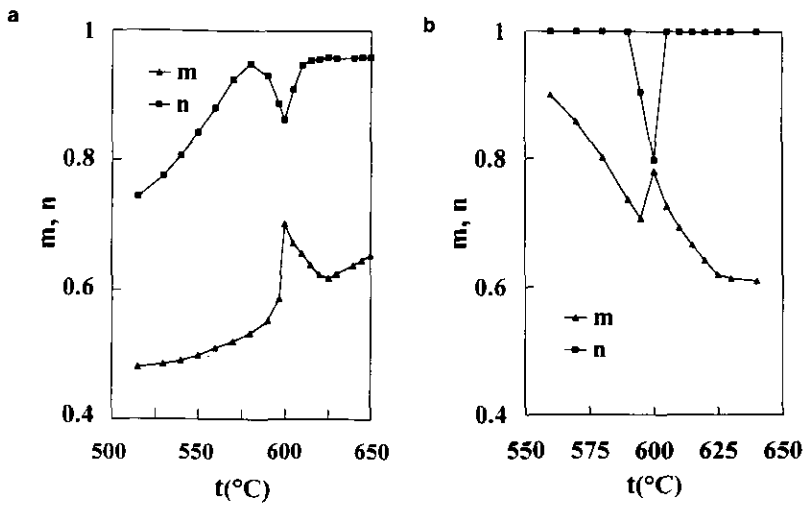

FIG. 7. Variation with temperature of the exponents m and n for (a) sample 1 and (b) samples 2 (the curves drawn through the reported data are visual guides).

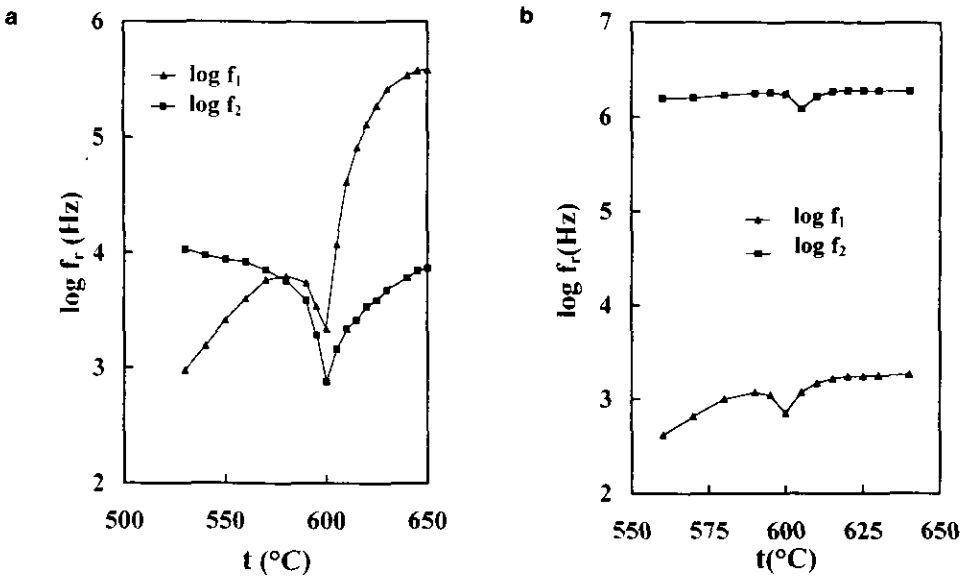

FIG. 8. Variation with temperature of the relaxation frequencies f_1 and f_2 for (a) sample 1 and (b) sample 2 (the curves drawn through the reported data are visual guides).

peak in ε_s at T_C for sample 2 probably results from a small deviation in crystal orientation; i.e., the surface of sample 2 is not exactly perpendicular to the a-axis.

On the other hand, the ε_∞ values, calculated for both samples, attain values of about 10^2 in the temperature range considered.

4.3. *Dielectric Permittivity* ε_r'

Equations [6] and [7] emphasize that ε_r' and ε_r'' consist of two parts: the lattice response $[(\varepsilon_r')_{latt}, (\varepsilon_r'')_{latt}]$ and the charge carrier contribution $[(\varepsilon_r')_{carr}, (\varepsilon_r'')_{carr}]$. Plots of log $(\varepsilon_r')_{latt}$ and log $(\varepsilon_r'')_{latt}$ with log f are given at the Curie point in Figs. 5a and 5b for samples 1 and 2.

The temperature dependences of $(\varepsilon_r')_{latt}$ and $(\varepsilon_r')_{carr}$ for sample 1 are shown in Fig. 10 at two frequencies, i.e., 10 and 10^3 Hz. As shown, even for the crystal oriented

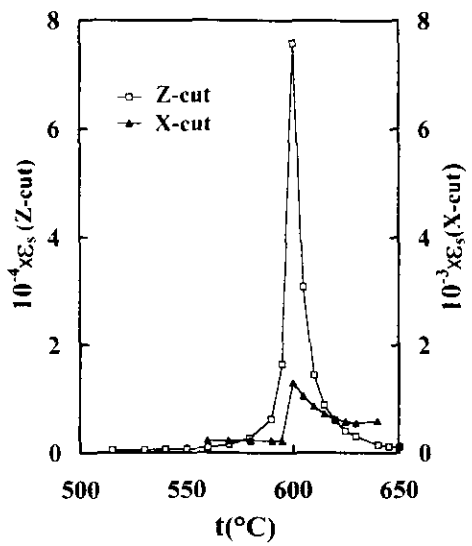

FIG. 9. Temperature dependence of the static permittivity, ε_s, for both samples (the curves drawn through the reported data are visual guides).

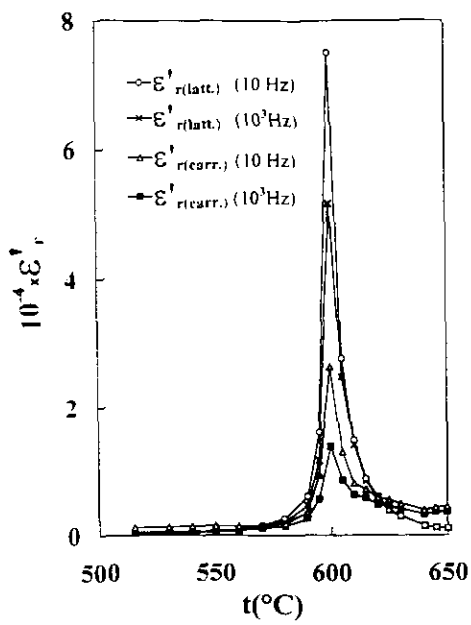

FIG. 10. Variation with temperature of $(\varepsilon_r')_{latt}$ and $(\varepsilon_r')_{carr}$ at 10 and 10^3 Hz for sample 1 (the curves drawn through the reported data are visual guides).

along the polar axis, the contribution of the charge carriers to the total permittivity is quite significant and increases with decreasing frequency; e.g., at 600°C the $(\varepsilon_r')_{carr}/(\varepsilon_r'')_{latt}$ ratio is equal to 0.26 (10^3 Hz) and 0.35 (10 Hz).

5. CONCLUSIONS

Based on ac impedance measurements, we have analyzed low-frequency dispersion phenomena in $Li_{0.980}Ta_{1.004}O_3$ single crystals oriented along and perpendicularly to the c polar axis in the 500–650°C temperature range around T_C.

Two contributions to the dielectric permittivity have been identified; one represents the lattice response and the other, the charge carrier response. The relaxation frequencies are minimal at the Curie temperature T_C, suggesting both mechanisms to be correlated with the soft mode. Both phenomena are related to Li atom motions.

A dielectric response relation has been proposed which may be considered a generalization to the Cole–Cole dielectric expression. The relation has been employed subsequently to determine the various dielectric parameters associated with both polarization mechanisms and to investigate their variation with temperature.

The influence of the charge carrier contribution on the dielectric permittivity is significant, as demonstrated when both lattice and carrier polarization mechanisms are simultaneously considered.

REFERENCES

1. K. S. Cole and R. H. Cole, *J. Chem. Phys.* **9,** 341 (1941).
2. J. Ravez and F. Micheron, *Actual. Chim.* **1,** 9 (1979).
3. R. L. Barns and J. R. carruthers, *J. Appl. Crystallogr.* **3,** 395 (1970).
4. A. Huanosta and A. R. West, *J. Appl. Phys.* **61,** 5386 (1987).
5. I. M. Hodge, M. D. Ingram, and A. R. West, *J. Electroanal. Chem.* **74,** 125 (1976).
6. D. P. Almond and A. R. West, *Solid State Ionics* **23,** 27 (1987).
7. J. A. Nelder and R. Meads, *Comput. J.* **7,** 308 (1965).
8. J. L. Servoin and F. Gervais, *Solid State Commun.* **31,** 387 (1979).
9. M. E. Lines and A. M. Glass, "Principles and Applications of Ferroelectrics and Related Materials." Clarendon Press, Oxford, 1977.
10. A. K. Jonscher, *Nature* **267,** 673 (1977).